Wave Height Estimation and Validation Based on the UFS Mode Data of Gaofen-3 in South China Sea

Limin Cui, Mingsen Lin, *Member, IEEE*, Youguang Zhang, and Yongjun Jia

***Abstract*—The ultrafine strip (UFS) of the Gaofen-3 (GF-3) satellite provides extensive ocean wave details due to the high spatial resolution of 3 m. In this article, a new empirical model is developed to estimate wave height from GF-3 UFS mode data in South China Sea (SCS). Traditional methods either have more input parameters or complex forms or complex transformations, and most of them depend on the visible wave pattern. The model has the advantages of fewer input parameters and unnecessary visual wave patterns. The wave height estimation model is developed based on the collated data pairs between GF-3 UFS data in horizontal-horizontal polarization and the ERA5 reanalysis dataset from 2018 to 2021. The datasets are randomly divided into two groups. One group (about 80%) is used to develop the empirical relation; the other group (about 20%) and some altimeter data are used for significant wave height (SWH) verification. The comparison of the model data with the remaining ERA5 (ECMWF Reanalysis v5) data and the altimeter shows that the root-mean-square error is 0.41 and 0.47 m, the scatter index is 29.24% and 29.79%, and the correlation coefficient is 0.90 and 0.82, respectively. These statistical indices suggest that the developed model is suitable for SWH retrievals. So, the study results indicate that the GF-3 UFS mode data provide valuable information about wave conditions in the SCS.**

***Index Terms*—ERA5 reanalysis, Gaofen-3 satellite, synthetic aperture radar (SAR), South China Sea (SCS), wave height.**

I. Introduction

THE South China Sea (SCS) is the largest semi-enclosed Sea in the western tropical Pacific ocean, and the ocean dynamic conditions are complex [1]. Among which ocean wave exerts significant impacts on marine activities and scientific applications. Wang *et al.* [2] think ocean wave is very important for fishing, shipping and oil platform safety. Stopa *et al.* [3] think the error of wind speed retrieved by *C*-band radar is mainly comes from the Sea state. Li *et al.* [4] confirmed that the wind speed inversion from Sentinel-1 wave mode (WM) is affected by waves. Significant wave height (SWH) is an essential parameter that can be used to describe ocean waves; its measuring and monitoring are of great significance [5].

As we all know, synthetic aperture radar (SAR) images contain some information related to ocean waves [6], [7], and has been widely used to observe ocean wave from space since the SEASAT was launched in 1978 [8].

Various wave extraction algorithms from SAR images have been investigated over the past decades. The first type of algorithm is based on the linear or non-linear approximation model to retrieve wave directional spectrum according to the visible wave pattern in SAR images [6], [7]. Subsequently, the technology is continuously improved based on the SAR ocean imaging theory, which has made great contributions to extracting wave directional spectrum from SAR images [9]–[11].

The second type of algorithm is the pure empirical algorithm. These algorithms obtain wave height information directly from SAR images and their statistics and spectra features. This technology was first applied to the ERS2 data (1996–1999) by Schulz-Stellenfleth, and it is later known as CWAVE_ERS [12]. After this, more models have been developed for C-band SAR satellites such as ERS-1 SAR [12], [13], Radarsat-2 [21], Envisat ASAR (Advanced SAR) [15], Sentinel-1 SAR [14], [16], and GF-3 SAR [17]–[21]. Meanwhile, some algorithms are also established for *X*-band SAR products, such as TerraSAR-x/TanDEM-X data [22]–[24].

The last type of algorithm is related to Artificial Intelligence (AI) and relies only on SAR images without any other information or transformation of the wave spectrum. These algorithms have been developed very rapidly for wave inversion in recent years. The backpropagation neural network (BPNN) was used by Wu *et al.* [25] and Stopa and Mouche [26] to extract SWH based on Sentinel-1 WM data. The deep learning method has also been used to retrieve wave parameters from SAR images [27]. The convolutional neural network was applied to Sentinel-1 image in VV polarization for SWH estimation by Xue *et al.* [28] . Evdokia *et al.* [29] predicted sea-state in an offshore wind farm based on machine learning techniques. Gao *et al.* [31] established the SWH retrieval model based on the support vector machine in an ASAR WM.

GF-3 is a satellite equipped with a space-borne quad-polarization *C*-band SAR with a spatial resolution of 1 to 500 m [32]. It was launched by the China Academy of Space Technology on August 10, 2016 [33]. Based on GF-3 data, a wide range of application, such as ocean wave, marine wind, oil spill, and ship detection, was carried out [34]. The GF-3 satellite has twelve imaging modes. Among them, GF-3 UFS mode data has a resolution of 3.0 m. Because of its higher resolution, GF-3 UFS mode data has a broad application scope, and it can obtain details of waves in ocean wave observation.

Manuscript received December 31, 2021; revised February 16, 2022; accepted March 5, 2022. Date of publication March 18, 2022; date of current version April 19, 2022. This work was supported in part by Key Special Project for introduced Talents Team of Southern Marine Science and Engineering Guangdong Laboratory (Guangzhou) under Grant GML2019ZD0303 and in part by the Special Program of Hainan Province for Academician Innovation Platform under Grant YSPTZX202002. *(Corresponding author: Limin Cui.)*

The authors are with the National Satellite Ocean Application Service, Beijing 100081, China (e-mail: cuilimin2021@126.com; mslin@mail.nsoas.org.cn; zhangyouguang@mail.nsoas.org.cn; jiayongjun@mail.nsoas.org.cn).

Digital Object Identifier 10.1109/JSTARS.2022.3160516

TABLE I
MAIN PARAMETERS FOR GF-3 UFS MODE

Mode	Pol	Res	Swath	Total
UFS	HH	3.0 m	30 km*30 km	1580

In this article, a new model is developed to estimate the SWH from high-resolution SAR data without the necessary visual wave pattern. Our method is motivated by the CWAVE_S1-IW algorithm developed by Pleskachevsky *et al.* [14]. The difference is that our method has the advantages of fewer input parameters and unnecessary wave-pattern.

The rest of this article is organized as follows. Section II presents all data used in this article. Section III describes the strategy of extracting the SWH. Section IV gives the validation results. Finally, Section V concludes this article.

II. DESCRIPTION OF THE DATA SOURCES

The level 1A product (single look complex) from the GF-3 UFS mode data, altimeter, and ERA5 reanalysis ocean wave and ocean wind dataset (hereinafter ERA5) are used in our study. A total of 1185 matched dataset between GF-3 images and the wave data and wind data from ERA5 are obtained. The dataset is randomly divided into two parts. To establish the wave retrieval model, about 1262 UFS mode SAR images are used for training. To independently validate the developed functions, the wave height from altimeter products and the remaining wave data from ERA5 are used. The data used for modeling and validating are described later.

A. GF-3 UFS Mode Data

The GF-3 is a sun-synchronous satellite [39]. Our study is based on GF-3 UFS mode data with HH polarization (*H* polarization for transit and *H* polarization for receive) acquired in SCS from 2018 to 2021. The data has a resolution of 3.0 m, and its swath is 30 km $\times$ 30 km. The descriptions of these collected UFS mode data are given in Table I. The location of the entire GF-3 data of the SCS is illustrated in Fig. 1. It can be seen that there are GF-3 data in most areas, and more data exists in the near-land area than in other areas. Fig. 2 presents the distribution of the incident angle for all selected SAR data. It is shown that the collected data has a wide range of incidence angles (19°–50°), and they are evenly distributed except around 35° and 45°.

B. ERA5 Reanalysis Dataset

ERA5 is the fifth-generation ECMWF (European Centre for Medium-Range Weather Forecasting) atmospheric reanalysis dataset of the global climate covering the period from January 1950 to the present. ERA5 is freely available through the EU-funded Copernicus Climate Change Service (C3S).[1] More detailed information about ERA5 can be found by Hersbach *et al.* [35]. In this article, the ERA5 hourly wave height and wind speed products are downloaded on the grid for the four-year period from January 1, 2018 to December 31, 2021. The wind dataset has a horizontal resolution of approximately 0.25°, and the wave dataset provides a spatial resolution of 0.5°.

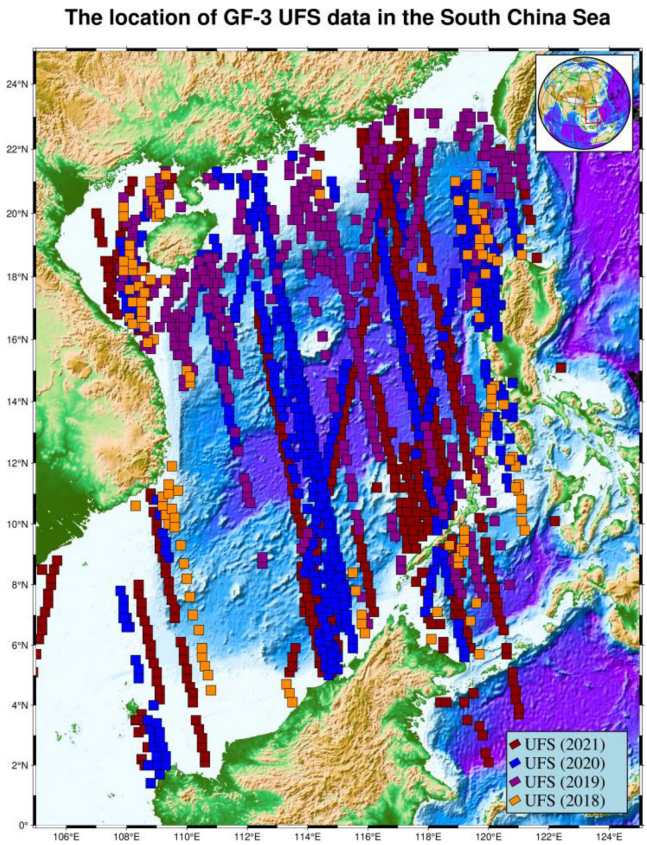

Fig. 1. Locations of all available GF-3 SAR images acquired in UFS mode. The dark red color, blue color, the magenta color, and the dark orange color stand for the data in 2021, 2020, 2019, and 2018.

The ERA5 wave and wind products in SCS have been evaluated in recent years. Shi *et al.* [36] evaluated the accuracy of the ERA5 wave reanalysis dataset by the buoy between January and December 2018 in northern SCS. They found that the SWH between the ERA5 dataset and buoy data shows a good correlation (correlation coefficient = 0.97) with a root-mean-square error (RMSE) of 0.14 m. Besides, the comparisons of the multiplatform wind products in the SCS based on the summer and autumn data of 2019 revealed that the RMSEs of ERA5 wind speed and wind direction are around 1.9 m s^{-1} and 33°, respectively [37]. It can be seen that the wind and wave products from ERA5 in the SCS have relatively high accuracy. So, it is feasible to choose the ERA5 reanalysis dataset to develop the wave retrieved model.

C. SWH Data from Radar Altimeters

Space-borne radar altimeters (RA) are another remote-sensing SWH instrument.Ribal and Young suggested that the wave height from the altimeter generally is more accurate than the SAR-derived SWH [38]. In this article, the altimeter L2 geophysical data records for SARAL/Altika, HY-2B, Jason-3, CFO (CFOSAT), Cryosat-2 and Sentinel-3a/b are used for model validation.

[1][Online]. Available: https://climate.copernicus.eu/

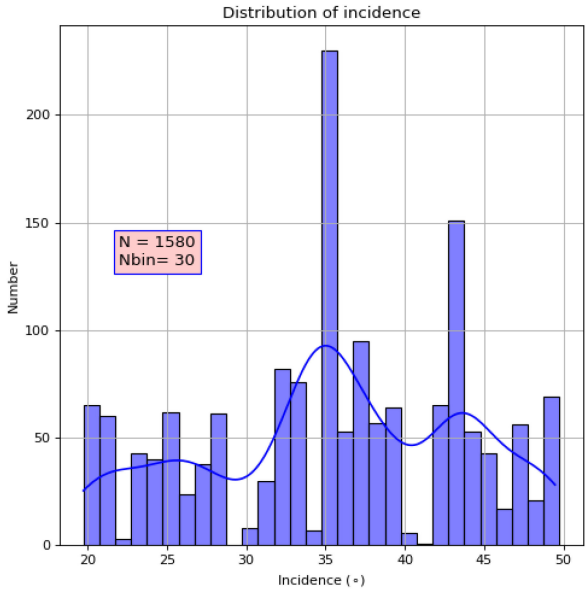

Fig. 2. Histograms of incidence for the entire UFS mode data.

III. Development of Empirical Wave Retrieval Model: CWAVE_GF3_UFS

A. Radio Calibration

The SAR products with high radiation accuracy are necessary for ocean wave inversion. For GF-3 SAR operating modes, the radiometric accuracy of normalized radar cross section (NRCS) is about 1.4 dB (3 σ), and that of noise equal sigma zero is between -20 dB and -22 dB [39].

The NRCS of GF-3 level 1A mode data is acquired by formula

$$\sigma^0 = DN^2 \left(\frac{M}{65535}\right)^2 - N\,[dB] \tag{1}$$

where σ^0 is the NRCS (unit: dB); DN is SAR-measured intensity; M and N are, respectively, the external calibration factor and the calibration constant, and they are stored in the annotation file.

B. Preprocessing

All ocean phenomena and marine targets including slicks, atmospheric gravity waves, current, oceanfront, thunderstorms, ships, and oil platforms can be imaged by SAR. These phenomena affect the detection of ocean waves due to their uneven and strong signals. Also, if the SAR data has a low signal or poor signal-to-noise ratio (SNR), wave parameters are difficult to estimate. In this article, the following criteria are used to reduce the impact of these factors on model development.

1) Homogeneity Check: Here, the normalized variance ($c$var) is calculated from SAR image intensity. The method recommended by Stopa and Mouche is adopted to limit the normalized variance within 1.0 to 2.0 [16]. The calculation formula of normalized variance is shown as

$$c\text{var} = \text{var}\left(\frac{I - \bar{I}}{\bar{I}}\right) \tag{2}$$

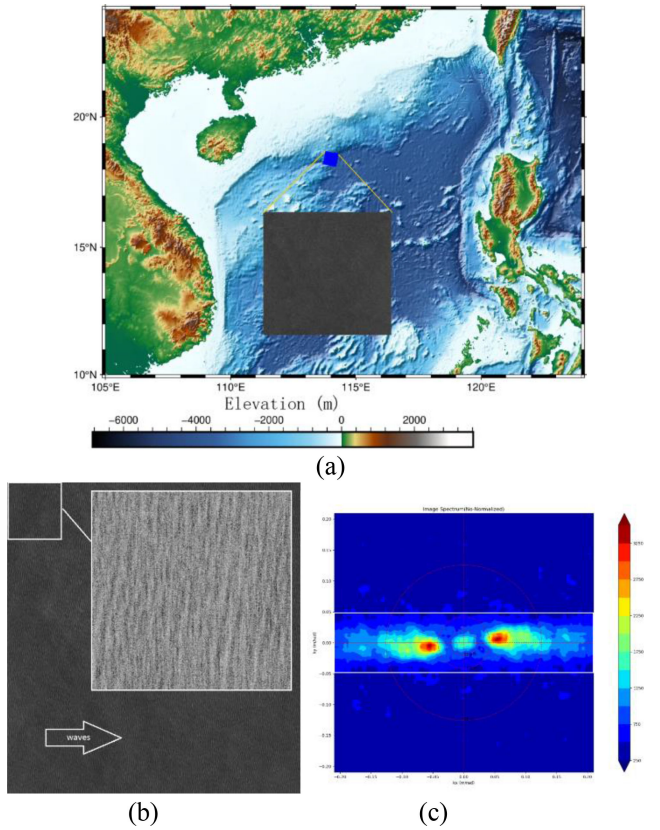

Fig. 3. GF-3 HH polarization UFS mode image in northern SCS at 10:39 UTC on 30 February 2019. (a) Presents the location of this image. (b) Presents the subimage (1024 × 1024 pixels = >3.0 km × 3.0 km). (c) Presents the image spectra.

where I is the mean intensity of the sub-image from the GF-3 UFS data in HH polarization.

2) Typhoon Data: The data during typhoons are rejected, due to the complexity of the Sea surface. The typhoon track dataset is used to eliminate the SAR data affected by the typhoon [40]. And the data within 400 km from the typhoon center was removed.

3) Low Signal-To-Noise Ratio: The data with wind speed less than 3.0 m s^{-1} or wave height less than 0.3 m are removed, due to low SNR.

In addition, the subimages with strong backscatter (such as ships, oil platforms, and rain cells) are rejected by visual inspections.

C. CWAVE_GF3_UFS Model

The previously developed empirical wave retrieval algorithms for SAR data include many input parameters. In this section, the wave height estimation model is developed based on the GF-3 UFS mode data through the input parameter combination test. The wave height is directly derived from the SAR image spectra, statistics of SAR images, and wind speed without transformation into wave spectra. The SAR image spectrum is calculated with a two-dimensional (2-D) fast Fourier transform. Fig. 3 shows an example of a quick view of a GF-3 HH polarization UFS image, which was imaged in Northern SCS at 10:39 UTC on January 30, 2019. The image with a white border is a view of

the subimage. The image spectra estimated from the subimage of the example is also presented in this figure.

The wave height estimation method recommended by Pleskachevsky *et al.* [14] is adopted in this article. The general form of this method is as follows:

$$H_s^{C\text{WAVE\_UFS}} = a_1 \sqrt{B_1 E_s \tan\theta} + \sum_{i=2}^{N} a_i B_i + C \quad (3)$$

where a_i denotes coefficients; θ is radar incidence angle; E_s is evaluated from 1024 $\times$ 1024 pixel sub-image from GF-3 UFS mode data in wavenumber space; B_i denotes correction terms; the square-root term $a_1\sqrt{B_1 E_s \tan\theta}$ relates the ocean wave to energy in the image spectra. According to the relation of SWH estimation from ocean wave spectra E_{ws}, $H_S = 4.0\sqrt{E_{\text{ws}}}$ ($a_1 = 4.0$). The parameter B_1 is a scaling factor related to the SAR image spectrum energy, which gives the non-linearity of the SAR imaging ocean waves. $B_1 = K_1 \times E_S^{100}/E_S^{600}$ is a relation between E_S^{100} with a wavelength of 30–100 m (noise is generally considered to exist in this spectral domain) and E_S^{600} with a wavelength of 100–600 m [14], [23]. B_2 is wind speed, which is the result of SAR inversion or external wind products, such as forecast data. The constant C is fitted using ERA5 reanalysis data.

The term with $i = 3 \sim n$ presents the statistics of the subimage, such as skewness and kurtosis, cvar, standard root difference, and mean value of NRCS. The skewness and kurtosis of NRCS of the subimage are calculated as follows [16]:

$$\overline{\sigma_0} = \frac{\sum_{i=0}^{n} \sigma_{0i}}{n} \quad (4)$$

$$\text{std} = \sqrt{\frac{\sum_{i=1}^{n} \left(\sigma_{0i} - \overline{\sigma_0}\right)^2}{n-1}} \quad (5)$$

$$\text{skew} = \frac{1}{n} \sum_{i=1}^{n} \left(\sigma_{0i} - \overline{\sigma_0}\right)^3 / s^3 \quad (6)$$

$$\text{kurt} = \frac{1}{n} \sum_{i=1}^{n} \left(\sigma_{0i} - \overline{\sigma_0}\right)^4 / s^4 \quad (7)$$

where s is the standard deviation of σ_0, $\overline{\sigma_0}$ is mean value of all data in subimage, and n is the total number of σ_0.

D. Development of the Empirical Model

Based on the GF-3 UFS mode data, the development of the SWH estimation model is shown in Fig. 4.

The developing strategy of the model is introduced as follows. First, a set of matched data pairs is obtained by using the spatio-temporal interpolation method. The ERA5 hourly data before and after the GF-3 observation time is interpolated bilinearly to the location of the GF-3 SAR image. Then, the wave height and wind speed are linearly interpolated to the GF-3 observation time. About 80% of the collocated data between GF-3 and ERA5 are used as training samples (1262 collocations) to develop the model, and the remaining data (318 collocations) and some RA wave height product constitute the validation dataset.

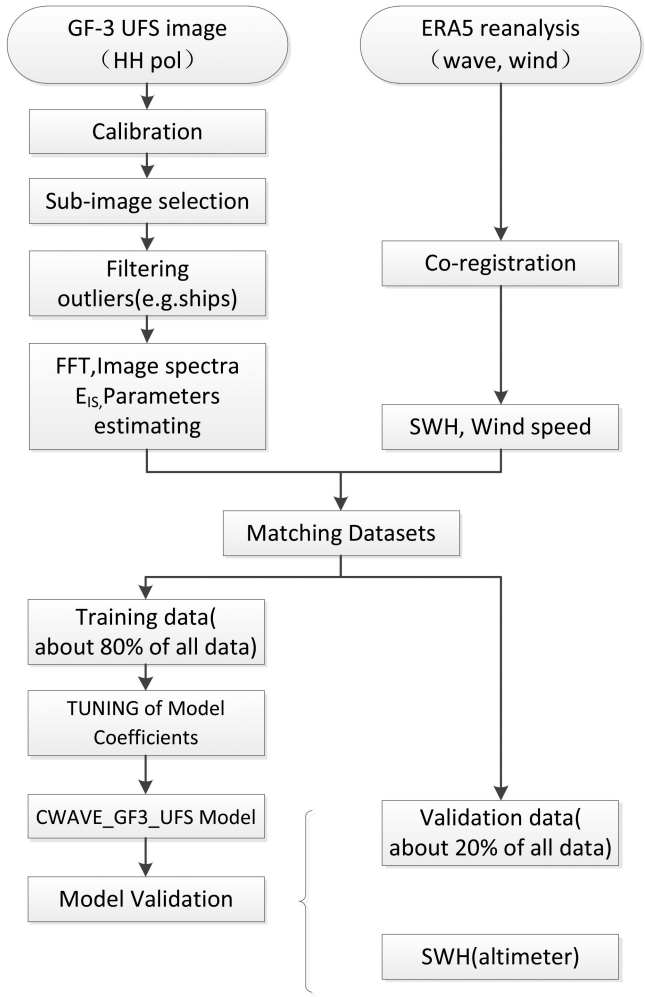

Fig. 4. Flowchart of developing the SWH estimation model.

To quantitatively evaluate the performance of the SWH estimation model under different input parameter combinations, several statistical metrics are applied to the validation dataset, including mean square error (MSE), RMSE, correlation coefficient (COR), and scatter index (SI). These statistical metrics are calculated through the following formulas:

$$\text{MSE} = \frac{1}{n} \left(y_i - x_i\right)^2 \quad (8)$$

$$\text{RMSE} = \sqrt{\frac{1}{n} \sum_{i=1}^{n} \left(y_i - x_i\right)^2} \quad (9)$$

$$\text{COR} = \frac{\sum_{i=1}^{n} \left(y_i - \bar{y}\right)\left(x_i - \bar{x}\right)}{\sqrt{\sum_{i=1}^{n} \left(y_i - \bar{y}\right)^2} \sqrt{\sum_{i=1}^{n} \left(x_i - \bar{x}\right)^2}} \quad (10)$$

$$\text{SI} = \frac{1}{\bar{x}} \sqrt{\frac{1}{n} \sum_{i=1}^{n} \left[\left(y_i - \bar{y}\right) - \left(x_i - \bar{x}\right)\right]^2} \quad (11)$$

where x and y indicate model observation and inversion values of the SWH, respectively [16]; the overbar denotes the mean, and n denotes the number of data pairs.

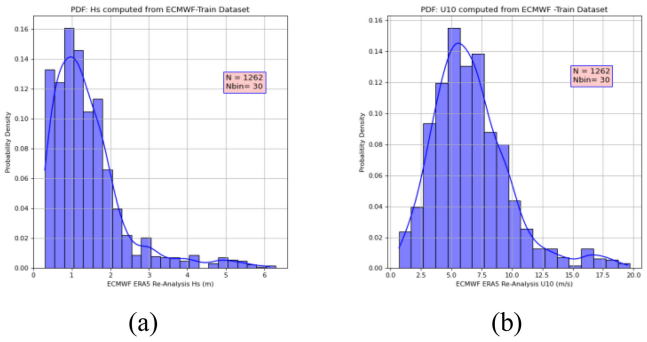

Fig. 5. Histogram of the SWH (left) and the wind speed (right) for the collected images.

TABLE II
SWH ERROR METRICS FOR DIFFERENT VARYING INPUT PARAMETERS

Model	Nn	MSE(m)	RMSE(m)	SI (%)	COR
$F(E)$	1	0.67	0.82	47.59	0.54
$F(E, spd)$	2	0.21	0.46	26.98	0.88
$F(E, spd, cvar)$	3	0.21	0.46	26.96	0.88
$F(E, spd, std)$	3	0.19	0.44	25.71	0.89
$F(E, spd, kurt)$	3	0.20	0.45	26.16	0.89
$F(E, spd, skew)$	3	0.21	0.45	26.44	0.88
$F(E, spd, mean)$	3	0.19	0.44	25.63	0.89
$F(E, spd, cvar, std, mean)$	5	0.19	0.44	25.42	0.89
$F(E, spd, std, mean)$	4	0.19	0.44	25.44	0.89
$F(E, spd, std, skew, mean)$	5	0.19	0.43	25.09	0.90
$F\left(\begin{matrix}E, spd, cvar, std, kurt, skew \\ , mean\end{matrix}\right)$	7	0.18	0.43	25.07	0.90

Fig. 5 presents a histogram of the ERA5 SWH (a) and wind speed (b) in the training dataset. It can be seen that the data in the low to moderate wave height is more than that in the high wave height. The SWH is between 0.3 and 6.4 m, and the wind speed ranges from 0.3 to 20 m s^{-1}.

The coefficients of the model are derived by linearly fitting based on the combination of different input parameters. The statistical metrics of different methods are given in Table II. It can be seen that both wind speed and spectral energy have a strong correlation with ocean wave height. Thus, these two parameters should be selected in the wave inversion model.

Next, several other parameters are considered. When the standard deviation and the mean value of NRCS are taken as input parameters for the training model, the value of the SI and the magnitude of correlation are improved. Therefore, these two parameters are also selected.

In addition, based on the method suggested by Stopa and Mouche the skewness and the kurtosis are tested, and the result is consistent with the conclusion in the literature (see details in [16]). In our model, skewness is used as the input parameter. Based on the above analysis, a total of five parameters are used in the proposed wave height estimation model (see the red box marked in Table II).

By fitting the scatters of the collocated data, the model coefficients are derived and given in Table III. The result shows that the ERA5 reanalysis wave and model data are highly correlated, with a correlation coefficient of 0.90.

TABLE III
MODEL COEFFICIENTS AND SWH ERROR METRIC

N	a0	a1	a2	a3	a4	a5	const	RMSE(m)
1262	4.0	0.1195	0.2298	-0.5668	-0.9337	-0.0466	-1.0021	0.43

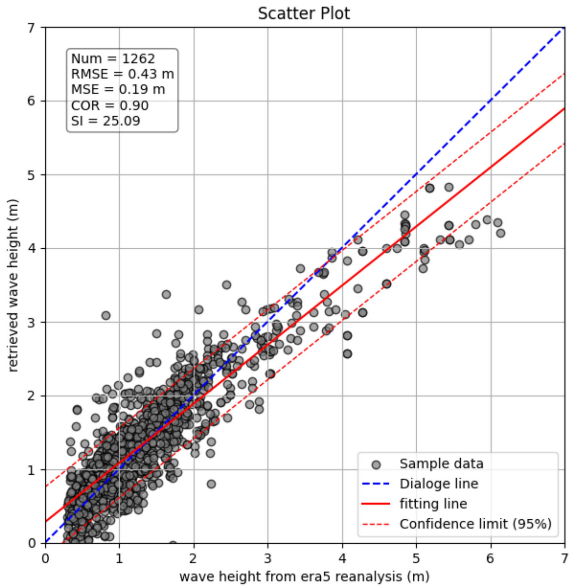

Fig. 6. SWH comparison of ERA5 and developed empirical functions. The blue dashed line represents the diagonal line; the solid red line represents the least-square linear regression result, and the dashed lines represent 95% of the data.

Fig. 6 shows a MSE of 0.19 m, an RMSE of 0.43 m, and an SI of 25.09%, which indicates that the SWH estimation from the developed model is equivalent to that given by ERA5 reanalysis. Thus, the developed empirical model has a good performance. Besides, it can be seen that the retrieved SWH is lower than the ERA5 data when the SWH exceeds 2.0 m. Moreover, the underestimation increases with the increase of the ocean wave height. The results in Table II and Fig. 6 show that the error of the retrieved SWH on the GF-3 SAR UFS-mode data is acceptable. In addition, our algorithm has the advantages of fewer input parameters and unnecessary visual wave patterns.

IV. VALIDATION AND DISCUSSION

A. Comparison With Wave Height From Remaining Datasets

The remaining ERA5 reanalysis wave data are used to verify the developed model. The scatter plot is given in Fig. 7. It can be seen that the inversion method achieves better performance for wave height estimation. Also, the wave height is underestimated for waves higher than 2.0 m. It may be because there are fewer wave height data above 2.0 m during the training process, which affects the estimation of SWH.

Some statistic characters, such as mean wave height, SI, and RMSE, are given in Table IV. These statistical metrics are analyzed according to different Sea states (0.39 m for SWH$<$2.0 m and 0.52 m for SWH$>$2.0 m). It can be found from Table IV

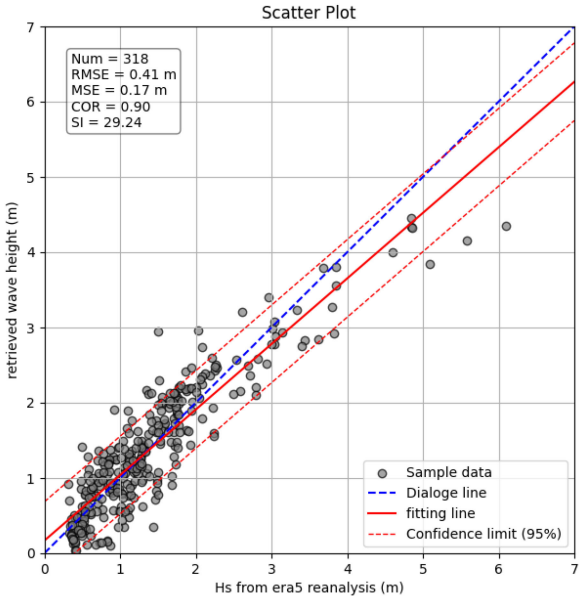

Fig. 7. Comparison of the wave height extracted on the GF-3 UFS data against ERA5 reanalysis data. The blue dashed line represents the diagonal line; the solid red line represents the least-square linear regression result, and the dashed lines represent 95% of the data.

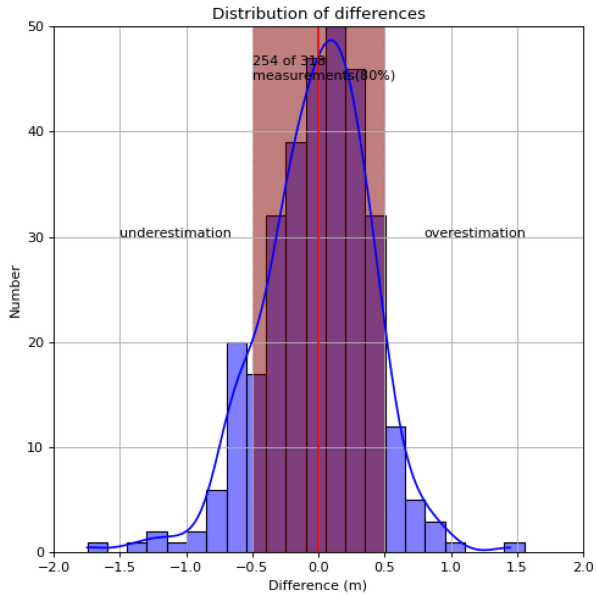

Fig. 8. Histogram of the underestimation and overestimation.

TABLE IV
ACCURACIES OF SWH ESTIMATION FOR DIFFERENT RANGES OF SWH

	SWH interval(m)	
Parameter	$0 < \text{SWH} < 2$	$2 < \text{SWH}$
RMSE(m)	0.39	0.52
SI	36.11	16.21
H_s^{mean}	1.07	3.04

that the RMSE increases a little as SWH increases, and the SI improves for a higher Sea state.

Further, the error distribution (only refers to RMSE) is also shown in Fig. 8. It can be seen that underestimation and overestimation are distributed on both sides of the 0 value. The vertical red line corresponds to zero bias. The absolute differences between the SWH from the ERA5 reanalysis wave data and that estimated from model are presented in the bins of 50 cm. Besides, the range of ± 50 cm contains 80% cases, which indicates that the accuracy of most inversion SWH is within 50 cm. Moreover, when using this model to estimate the wave height, there are more overestimated cases than underestimated cases.

B. Comparison With Wave Height From RA

In this section, the developed model is further evaluated with altimeter RA SWH data. Here, the temporal and spatial criteria of 1 h and 100 km are adopted. After spatial-temporal colocation processing, only Ka-band SARAL/ALtika, Ku-band HY-2B, Jason-3, Cryosat-2, and CFO could be co-located with GF-3 UFS mode data during our study period. The location of the collocated altimeter data is illustrated in Fig. 9. There are 208 pairs of matched data, including 42 from SARAL/ALtika, 8 from Jason-3, 66 from CFO, 42 from Cryosat-2 and 50 from HY-2B.

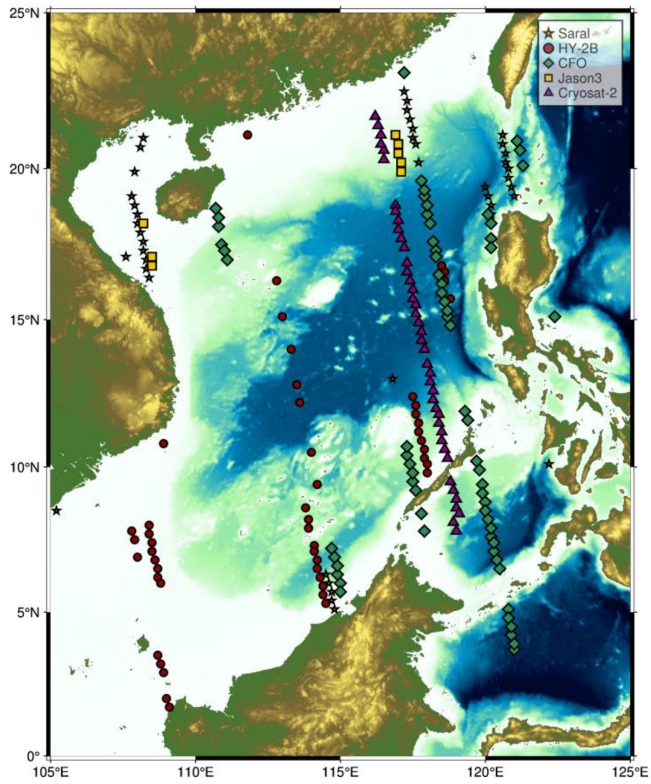

Fig. 9. Location of the collocated altimeter data.

The range of the collocated RA SWH is between 0.34 and 3.71 m.

Fig. 10 shows the comparison between the retrieved SWH from the GF-3 UFS mode data and the collocated RA wave products. The MSE is 0.24 m, the RMSE is 0.47 m, the SI is 29.79, and the COR is 0.82. These results are consistent with those presented in Fig. 7. Also, it can be seen that this model underestimates the SWH compared with the wave height of the

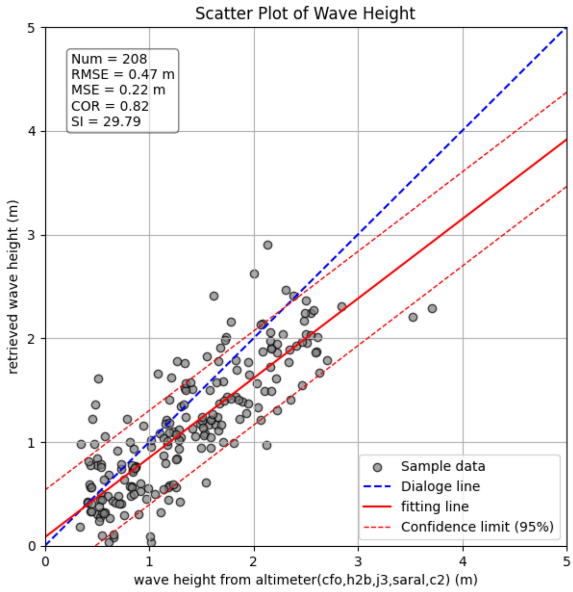

Fig. 10. Comparison of the wave height extracted on the GF-3 UFS data against the wave height from RA. The blue dashed line represents the diagonal line; the solid red line represents the least-square linear regression result, and the dashed lines represent 95% of the data.

altimeter. It can also be seen that the error increases with the increase of wave height, but the RMSE is acceptable.

In summary, our model has the RMSE of the developed model is 0.41 and 0.47 m, respectively, compared with remaining ERA5 reanalysis and altimeter wave products. The accuracy of other models in recent years is as follows. Li *et al.* [41] compared the wave height estimated from the ASAR WM data with buoys and numerical models, and gave the RMSE is 0.64 and 0.25 m, respectively. Wang *et al.* [20] represents that the RMSE about wave height using GF-3 WM data is between 0.50 and 0.60 m. Pleskachevsky *et al.* [14] estimated the SWH from *S*1 data in the North Sea and eastern Baltic Sea, and the RMSE is 0.80 m. Wu *et al.* [25] gives the RMSE of 0.71 m for SWH based on the *S*1 data in the arctic ocean using BPNN. Therefore, compared with the above model, our model has accepted accuracy.

V. Conclusion

Motivated by previous SAR-ocean wave empirical algorithms, this article presents an empirical model for estimating SWH on the SAR UFS mode data. The empirical function integrates radar incidence, the integrated energy of image spectrum, wind speed, and the mean, skewness, and standard deviation of images without necessary visual wave pattern.

The model is trained with ERA5 reanalysis data, and the model data are independently compared with the remaining ERA5 wave height and RA wave product. Experimental results indicate good inversion accuracy, with the RMSE of 0.41 m, the SI of 29.24%, and the COR of 0.90. The GF-3 retrieved SWH is further compared with RA, with the RMSE of 0.47 m, the SI of 29.79%, and the COR of 0.82. It can be seen from the verification results that the proposed model is suitable for wave height extraction from GF-3 UFS mode data in SCS, which improves SAR data application. It should be noted that some complex ocean wave data under typhoon conditions are not involved in this article, which needs further investigation in the future. In addition, it has an impact on the operation that the artificial filtering of the data, which contain rain or other clutters. Therefore, referring to the method given in [42], the automatic identification technique will be added to the operational wave height inversion model in future work.

References

[1] B. T. Xie, X. H. Ren, X. Jia, and Z. G. Li, "Research on ocean wave spectrum and parameter statistics in the Northern South China Sea," in *Proc. Offshore Technol. Conf.*, May 2019.

[2] H. Wang, D. Fu, D. Liu, X. Xiao, X. He, and B. Liu, "Analysis and prediction of significant wave height in the Beibu Gulf, South China Sea," *J. Geophys. Res. Oceans*, vol. 126, no. 3, Mar. 2021.

[3] J. E. Stopa, A. A. Mouche, B. Chapron, and F. Collard, "Sea state impacts on wind speed retrievals from C-band radars," *IEEE J. Sel. Topics Appl. Earth Observ. Remote Sens.*, vol. 10, no. 5, pp. 2147–2155, May 2017.

[4] H. Li, A. Mouche, and J. E. Stopa, "Impact of Sea state on wind retrieval from Sentinel-1 wave mode data," *IEEE J. Sel. Topics Appl. Earth Observ. Remote Sens.*, vol. 12, no. 2, pp. 559–566, Feb. 2019.

[5] J. Wang, L. Aouf, X. Wang, B. Li, and J. Wang, "Remote cross-calibration of wave Buoys based on significant wave height observations of altimeters in the northern hemisphere," *Remote Sens.*, vol. 12, no. 20, 2020, Art. no. 3447.

[6] W. Alpers, D. B. Ross, and C. L. Rufenach, "On the detectability of ocean surface waves by real and synthetic aperture radar," *J. Geophys. Res. Oceans*, vol. 86, no. 7, pp. 6481–6498, 1981.

[7] K. Hasselmann and S. Hasselmann, "On the nonlinear mapping of an ocean wave spectrum into a synthetic aperture radar image spectrum and its inversion," *J. Geophys. Res. Oceans*, vol. 96, no. 6, pp. 10713–10729, 1991.

[8] Y. He, H. Shen, and W. Perrie, "Remote sensing of ocean waves by polarimetric SAR," *J. Atmos. Ocean. Technol.*, vol. 23, no. 12, pp. 1768–1773, Dec. 2006.

[9] S. Hasselmann1, K. Hasselmann1, J. H. Allender, and T. P. Barnett, "Computations and parameterizations of the nonlinear energy transfer in a gravity-wave spectrum. Part II: Parameterizations of the nonlinear energy transfer for application in wave models," *J. Phys. Oceanogr.*, vol. 15, pp. 1378–1391, 1985.

[10] H. E. Krogstad, O. Samset, and P. W. Vachon, "Generalizations of the nonlinear ocean-SAR transform and a simplified SAR inversion algorithm," *Atmos. Ocean*, vol. 32, no. 1, pp. 61–82, 1994.

[11] B. Zhang, W. Perrie, and Y. He, "Validation of RADARSAT-2 fully polarization SAR measurements of ocean surface waves," *J. Geophys. Res. Oceans*, vol. 115, no. C6, 2010, Art. no. 2009JC005887.

[12] C. Mastenbroek and C. F. de Valk, "A semiparametric algorithm to retrieve ocean wave spectra from synthetic aperture radar," *J. Geophys. Res. Oceans*, vol. 105, no. 3, pp. 497–516, 2000.

[13] J. Schulz-Stellenfleth, T. Koenig, and S. Lehner, "An empirical approach for the retrieval of integral ocean wave parameters from synthetic aperture radar data," *J. Geophys. Res. Oceans*, vol. 112, pp. 3019–3033, 2007.

[14] A. Pleskachevsky, S. Jacobsen, B. Tings, and E. Schwarz, "Estimation of Sea state from Sentinel-1 synthetic aperture radar imagery for maritime situation awareness," *Int. J. Remote Sens.*, vol. 40, no. 11, pp. 4104–4142, Jan. 2019.

[15] X. M. Li, S. Lehner, and T. Bruns, "Ocean wave integral parameter measurements using ENVISAT ASAR wave mode data," *IEEE Trans. Geosci. Remote Sens.*, vol. 49, no. 1, pp. 155–174, Jan. 2011.

[16] J. E. Stopa and A. Mouche, "Significant wave heights from Sentinel-1 SAR: Validation and applications," *J. Geophys. Res. Oceans*, vol. 122, no. 3, pp. 1827–1848, Mar. 2017.

[17] Y. X. Sheng *et al.*, "Significant wave height retrieval from co-polarization Chinese Gaofen-3 SAR Imagery using an improved algorithm," *Acta Oceanol. Sinica*, vol. 37, pp. 1–10, 2018.

[18] W. Z. Shao, Y. X. Sheng, and J. Sun, "Preliminary assessment of wind and wave retrieval from Chinese Gaofen-3 SAR imagery," *Sensors*, vol. 17, no. 8, 2017, Art. no. 1705.

[19] J. Wang, H. Wang, W. Shao, J. Zhu, and X. Z. Yuan, "Significant wave height retrieval from Gaofen-3 wave mode images," in *Proc. IEEE Int. Geosci. Remote Sens. Symp.*, Jul. 2018, pp. 3204–3207.

[20] H. Wang *et al.*, "Empirical algorithm for significant wave height retrieval from wave mode data provided by the Chinese satellite Gaofen-3," *Remote Sens.*, vol. 10, no. 3, p. 363, 2018.
[21] L. Ren, J. S. Yang, G. ZH, and J. Wang, "The significant wave height estimation by the azimuth cutoff of the quad-polarization SAR image," *Proc. SPIE*, vol. 9261, 2014, Art. no. 926115.
[22] M. Bruck and S. Lehner, "TerraSAR-x/TanDEM-X Sea state measurements using the XWAVE algorithm," *Int. J. Remote Sens.*, vol. 36, no. 15, pp. 3890–3912, Jul. 2015.
[23] S. Lehner, A. Pleskachevsky, D. Velotto, and S. Jacobsen, "Meteo-marine parameters and their variability observed by high resolution satellite radar images," *Oceanography*, vol. 26, no. 2, pp. 80–91, 2013.
[24] A. Pleskachevsky, W. Rosenthal, and S. Lehner, "Meteo-Marine parameters for highly variable environment in coastal regions from satellite radar images," *J. Photogramm. Remote Sens.*, vol. 119, pp. 464–484, 2016.
[25] K. Wu, X. M. Li, and B. Q. Huang, "Retrieval of Ocean wave heights from spaceborne SAR in the Arctic Ocean with a neural network," *J. Geophys. Res. Oceans*, vol. 126, no. 3, 2021.
[26] J. E. Stopa and A. Mouche, "Significant wave heights from Sentinel-1 SAR: Validation and applications," *J. Geophys. Res. Oceans*, vol. 122, no. 3, pp. 1827–1848, Mar. 2017, Art. no. e2020JC016946.
[27] B. Quach, Y. Glaser, J. E. Stopa, A. A. Mouche, and P. Sadowski, "Deep learning for predicting significant wave height from synthetic aperture Radar," *IEEE Trans. Geosci. Remote Sens. Oceans*, vol. 59, no. 3, pp. 1859–1867, Mar. 2021.
[28] S. Xue, X. Geng, X. H. Yan, T. Xie, and Q. Yu, "Significant wave height retrieval from Sentinel-1 SAR imagery by convolutional neural network," *J. Oceanogr.*, vol. 76, no. 6, pp. 465–477, 2020.
[29] E. Tapoglou, M. F. Rodney, M. D. Robert, and D. Parsons, "Machine learning for satellite-based sea-state prediction in an offshore windfarm," *Ocean Eng.*, vol. 235, no. 1, 2021, Art. no. 109280.
[30] S. Shangguan, X. Qiu, K. Fu, B. Lei, and W. Hong, "GF-3 polarimetric data quality assessment based on automatic extraction of distributed targets," *IEEE J. Sel. Topics Appl. Earth Observ. Remote Sens.*, vol. 13, pp. 4282–4294, 2020.
[31] D. Gao, Y. X. Liu, J. M. Meng, Y. J. Jia, and C. Q. Fan, "Estimating significant wave height from SAR imagery based on an SVM regression modes," *Acta Oceanol. Sinica*, vol. 37, no. 3,pp. 103–110, 2018.
[32] H. Wang *et al.*, "Calibration of the copolarized backscattering measurements from Gaofen-3 synthetic aperture radar wave mode imagery," *IEEE J. Sel. Topics Appl. Earth Observ. Remote Sens.*, vol. 12, no. 6, pp. 1748–1762, Jun. 2019.
[33] Q. Chen, Z. Li, P. Zhang, H. Tao, and J. Zeng, "A preliminary evaluation of the Gaofen-3 SAR radiation characteristics in land surface and compared with Radarsat-2 and Sentinel-1A," *IEEE Geosci. Remote.*, vol. 15, no. 7, pp. 1040–1044, Jul. 2018.
[34] L. Zhao *et al.*, "China's Gaofen-3 satellite system and its application and prospect," *IEEE J. Sel. Topics Appl. Earth Observ. Remote Sens.*, vol. 14, pp. 11019–11028, 2021.
[35] H. Hersbach *et al.*, "The ERA5 global reanalysis," *Quart. J. Roy. Meteorol. Soc.*, vol. 146, no. 730, pp. 1999–2049, 2020.
[36] H. Shi *et al.*, "Evaluating the accuracy of ERA5 wave reanalysis in the water around China," *J. Ocean Univ. China*, vol. 20, pp. 1–9, 2021.
[37] Y. X. Liu, M. S. Lin, X. W. Jiang, X. J. Sun, and X. Z. Song, "A comparison of multiplatform wind products in the South China Sea during summer and autumn in 2019," *J. Oceanol. Limnol.*, vol. 39, pp. 2181–2194, 2021.
[38] A. Ribal and I. R. Young, "33 years of globally calibrated wave height and wind speed data based on altimeter observations," *Sci. Data*, vol. 6, 2019.
[39] Q. J. Zhang, "System design and key technologies of the GF-3 satellite," *Acta Geodaetica Cartographica Sinica*, vol. 46, pp. 269–277, 2017.
[40] X. Q. Lu *et al.*, "Western North Pacific tropical cyclone database created by the China Meteorological Administration," *Adv. Atmos. Sci.*, vol. 38, no. 4, pp. 690–699, 2021.
[41] X. M. Li, T. Koenig, J. Schulz-Stellenfleth, and S. Lehner, "Validation and intercomparison of ocean wave spectra inversion schemes using ASAR wave mode data," *Int. J. Remote Sens.*, vol. 31, no. 17/18, pp. 4969–4993, Sep. 2010.
[42] X. Chen and W. Huang, "Identification of rain and low-backscatter regions in X-band marine radar images: An unsupervised approach," *IEEE Trans. Geosci. Remote Sens.*, vol. 58, no. 6, pp. 4225–4236, Jun. 2020.

Limin Cui received the B.S. degree in surveying and mapping engineering from the China University of Petroleum, Dongying, China, in 2002, and the Ph.D. degree in physical oceanography from the Institute of Oceanology, Chinese Academy of Sciences, Qingdao, China, in 2010.

Since 2010, he has been with the National Satellite Ocean Application Service, Beijing, China, where he is currently an Associate Researcher. His current research interests include ocean surface waves and wind fields remote sensing by synthetic aperture radar and satellite image processing.

Mingsen Lin (Member, IEEE) received the B.S. degree in applied mechanics from the National University of Defense Technology, Changsha, China, in 1984, and the Ph.D. degree in computational mathematics from the Computing Center, Chinese Academy of Sciences, Beijing, China, in 1992.

He is currently the Chief Designer of the ground application system for Chinese salinity satellites, synthetic aperture radar satellites, and new generational ocean dynamic satellites. He was also a Deputy Chief Designer of the ground application system for the HY-1 and HY-2 satellites, where he organized the framework for the Chinese ocean satellite outline and managed the construction of the ground application system for the Chinese ocean satellite with the National Satellite Ocean Application Service, Beijing, China. He is one of the Founders of satellite ocean remote sensing in China. He plays an important role in the development of Chinese ocean satellites and manned space flight. His research interests include ocean satellite data processing, remote sensing of the ocean, and associated applications.

Youguang Zhang received the Ph.D. degree in ocean remote sensing fields from the Institute of Oceanology, Chinese Academy of Sciences, Beijing, China, in 2004.

He was the Deputy Chief of the Chinese HY-2 satellite ground system and the ocean salinity satellite ground system. He was a member of the marine satellite ground application system project. He has authored or co-authored more than 50 peer-reviewed papers on remote sensing. His research interests include satellite altimeter data processing and application research, satellite wave spectrometer data processing and application research, and the marine microwave remote sensor calibration technology research.

Yongjun Jia received the B.S. degree in information and computing science from Inner Mongolia University, Hohhot, China, and the M.S. and Ph.D. degrees in physical oceanography from the Institute of Oceanology, Chinese Academy of Sciences, Qingdao, China, in 2007 and 2010, respectively.

Since 2016, he has been an Associate Researcher with National Satellite Ocean Application Service, Beijing, China. His research interests include ocean microwave remote sensing and satellite oceanography.